Finite Element Analysis of Delamination in Woven Composites under Quasi-Static Indentation

M. C. Song[1], B.V. Sankar[1], G. Subhash[1], C. F. Yen[2]

Abstract: Delamination initiation and propagation in plain woven laminates and 3D orthogonal woven composites during short beam shear (SBS) test were analyzed using finite element (FE) analyses. Two kinds of 3D woven composites, containing single z-yarns and double z-yarns, were considered. The FE models were guided by experimental observations from SBS tests for the same material systems. A series of mechanisms including creation and evolution of matrix cracks and delaminations were modeled discretely. The force-displacement curves obtained from the FE simulations were compared with those from experiments. Further parametric studies were conducted to investigate the effects of z-yarns and interlaminar fracture toughness on delamination in woven composites. The results from the FE simulations revealed that z-yarns in 3D woven composites can play a major role in impeding propagation of interlaminar cracks. On the other hand 2D plain woven laminates without any z-reinforcement demonstrated higher interlaminar fracture toughness due to undulation in yarns. 3D woven composites with double yarns showed better damage tolerance than single yarn 3D woven composites and their behavior was very similar to composite laminates with high interlaminar fracture toughness.

Keywords: 3D woven composites, plain woven laminate, FEM cohesive element, delamination

1 Introduction

Prediction of damage and failure in laminated composite materials is one of the significant considerations in the design and operation of composite structures in various applications such as aerospace structures and military equipment. Among the various damage modes delamination is the most serious one as it leads to severe stiffness loss of the structures. Various methods for arresting crack growth

---

[1] University of Florida, Gainesville, FL, USA.

[2] US Army Research Laboratory, Aberdeen Proving Ground, MD, USA.

due to delamination have been suggested, e.g. [Sankar and Sharma (1997); Jain and Mai (1998); Chen, Sankar and Ifju (2002); Cartie (2000)]. One of those is to embed trans laminar reinforcements (TLRs) into the composite. Among several manufacturing processes used to include TLRs, 3D weaving process has substantial advantage over stitching or z-pinning in that the traditional weaving machines can be readily utilized. Numerous experimental [Sankar and Sharma (1997); Jain and Mai (1998); Chen, Sankar and Ifju (2002); Cartie (2000)], numerical[Cartie (2000); Dantuluri, Maiti, Geubelle, Patel and Kilic (2007); Grassi and Zhang (2003); Ratcliffe and Kruger (2006); Sankar and Hu(1991)] and analytical studies [Sankar and Dharmapuri (1998); Sridhar, Massabo, Cox and Beyerlein (2002); Ratcliffe and O'Brien (2004); Robinson and Das (2004); Mabson and Deobald (2000); Byrd and Birman (2005); Song, Sankar, Subhash and Yen (2012); Sankar and Zhu (2000)] have been conducted to determine the effect of TLRs on delamination of composites. Walter et al. [Walter, Subhash, Sankar and Yen (2010)] has tested different types of woven composites using short beam shear (SBS) test, and reported that the amount and type of z-yarns can influence the damage characteristics of composites.

Our goal in the present study is to evaluate the effect of z-yarn, on suppressing the delamination propagation and thus enhancing the damage tolerance of composites using finite element (FE) simulations. Resistance against crack development can be quantified by apparent fracture toughness expressed in terms of inherent interlaminar fracture toughness and the additional energy required due to bridging effect [Walter, et al., (2010)]. The influences of both these terms on delamination were analyzed using finite element method (FEM). We selected three different types of specimens; single and double yarn 3D woven composites, denoted as SY3W and DY3W, respectively, and 2D plain woven laminated composite (2DPL) for this study. The effects of z-yarn and inherent interlaminar fracture toughness on damage tolerance were investigated by comparing the load-deflection behavior SY3W and the DY3W to the 2DPL specimen and varying inherent interlaminar fracture toughness of the 2DPL in a parametric study.

It is well known that matrix cracks precede delamination when a laminated composite beam/plate is subjected to a quasi-static indentation or an impact load [Sankar and Sun (1986)]. Walter et al. [Walter, Subhash, Sankar and Yen (2010)] performed short beam shear tests on 3D woven glass/epoxy composites to understand the damage initiation and propagation mechanisms under impact loads. The experiments showed that matrix cracks initiated in resin pockets between the z-yarns and also in the weft yarns parallel to the *y*-axis (see Fig. 1). Optical micrographs also showed short delaminations and crushing failure beneath the indenter. However, these failures were highly localized beneath the indenter. On the other hand, the delaminations emanating from matrix cracks significantly changed the global

response of the specimens by reducing their stiffness significantly. In fact the interaction of matrix cracks and delaminations is a common feature typically observed in cross-ply laminated composites comprising of 0° and 90° unidirectional composite layers. Since orthogonally woven composites consist of warp yarns (0°) and weft yarns (90°) and the individual yarns can be treated as unidirectional composites, understanding of damage mechanisms in the latter can be useful in designing orthogonal woven composites. Although continuum damage models are suggested and able to capture the non-linear behavior of composites in certain situations, they are not suitable for modeling the discrete characteristics of damage process in the present study [Wisnom (2010)]. Hence the matrix cracks and delaminations are usually modeled discretely in order to study their interactions [Hallett, Jiang, Khan and Wisnom (2008); Zhou, Fang, Cox and Yang (2010)].
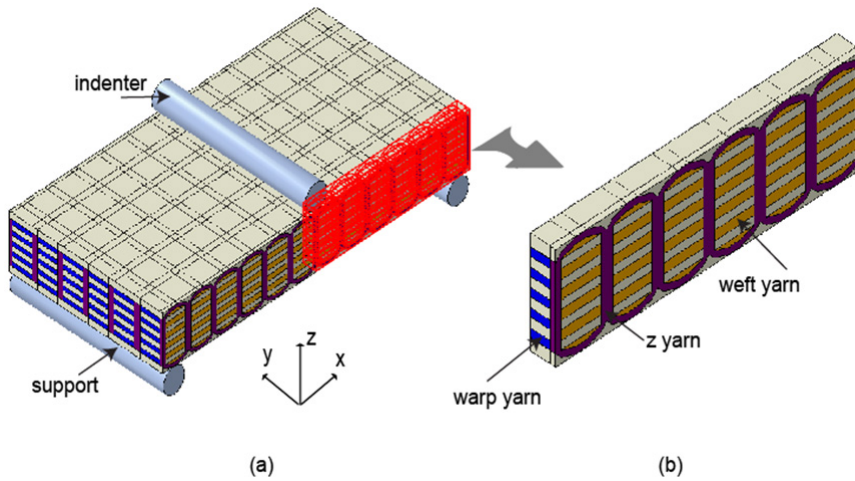

Figure 1: (a) Orthogonally woven 3D composite with the SBS setup and (b) Representative Volume Element (RVE) for the FE model

Cohesive elements are widely used for modeling of delaminations and matrix cracks because of their versatility in dealing with damage initiation and evolution without defining any pre-crack [Nishikawa, Okabe and Takeda (2007), Okabe and Yashiro (2012)]. Apart from delaminations which mostly occur at the interfaces between layers, the location and direction of matrix cracks may be arbitrary. The extended finite element method (X-FEM) [Belytschko, Cracie, and Ventura (2009)] and the augmented finite element method (A-FEM) [Ling, Yang and Cox (2009)] have been used to deal with these arbitrary discontinuities due to cracks in the material system. However, it might be difficult to predict exactly the creation of multiple cracks in

complex material systems such as woven composites as observed in the experiment without considering uncertainties in geometric configurations, internal defects or material properties. Our interest in the present study is focused on the investigation of delamination rather than exact prediction of intra-laminar damage attributes in the given material systems. Results from the SBS tests [Walter, Subhash, Sankar and Yen (2010)] provide good guidelines to predict the occurrence of matrix cracks. Then cohesive elements can be used in modeling matrix cracks as well as delaminations. The potential locations for matrix cracks were assumed based on the observation of SBS test specimens and their orientation was determined from the principal (tensile) stress direction in the study. It should be highlighted again that our intention in this paper is to clarify the role of z-yarns on delamination in 3D woven composites with different z-yarn volume fraction and a 2D plain woven composite.

The FE simulations were used to obtain the force-displacement relations of various 3D woven composites and to investigate the effect of z-yarns on the apparent interlaminar fracture toughness. The relationships between damage patterns and the global response observed in the SBS tests are also explained using the FE results.

2   Finite element model

2.1   3D woven composites

The microstructure of the specimens and their boundary conditions in the FE models were based on the experimental studies reported by Walter et al. [Walter, Subhash, Sankar and Yen (2010)]. The geometric parameters of the DY3W such as yarn dimensions and yarn spacing were determined from the micrographs of the 3D orthogonal woven composite [Walter, Subhash, Sankar and Yen (2010)] and summarized in Table 1. As shown in Figs. 1 and 2 the cross-sections of the yarns were treated as rectangles. Due to symmetry about the *yz*-plane passing through the mid-span, only one-half of the specimen in the *x*-direction was modeled. Since the specimen was assumed to be under a state of plane strain normal to the *y*-axis, one unit-cell in the width direction (*y*-direction) should be sufficient. Further reduction could be made as the unit-cell is symmetric about its mid-plane parallel to the *xz*-plane. Thus, only one half of the unit-cell needs to be considered as shown in Fig. 1(b). The indenter and supports of the SBS test setup were modeled as rigid bodies. The span of the beam (distance between the supports) in the FE model was 40 mm. The thickness of the z-yarn in the SY3W was 0.4 mm, half of that in the DY3W. Apart from altering the thickness of the z-yarn in the SY3W other geometric dimensions remained the same in the SY3W and the DY3W specimens. In addition, the regions created by reducing the thickness of the z-yarn were replaced by matrix

material since more matrix regions in the SY3W were observed in the micrograph of the specimens [Walter, Subhash, Sankar and Yen (2010)].

Table 1: Dimensions of geometric model of the RVE in mm units [17]. The subscripts x, y and z indicate warp yarn, weft yarn and z yarn, respectively.

L_s	w_z	t_x	t_y	t_z	w_y	t_g
1.8	0.4	0.5	0.6	0.8	2.8	0.075

Plane strain boundary conditions were assigned on the front and back surface of 3D woven composites ($x - z$ planes in Fig.1) as well as the symmetry boundary conditions on the symmetry plane such that U_x=0 (left $y - z$ plane in Fig.1). Eight-nodes brick elements were used in modeling the yarns and matrix phase and eight-node cohesive elements were used for damage modeling.

Considering linear elastic behavior of the yarns and matrix, elastic constants of the yarns were computed using the micromechanics formulas developed by Chamis et al. [Chamis, Handler and Manderscheid (2007)]. The yarns were comprised of S2 glass fiber (Elastic modulus of 86.9GPa and Poisson's ratio of 0.23) and SC-15 epoxy along with 62% fiber volume fraction. The strength and critical energy release rate values for the cohesive elements were selected from the literature [Walter, Subhash, Sankar and Yen (2010); Advanced Materials (2013); Huang and Waas; Applied Poleramic (2013)]. The material properties of the yarns, the epoxy and the cohesive elements used in the FE models are listed in Table 2.

Table 2: Material properties of the constituents in the 3D woven composites [27]

Yarns (Transversely isotropic)								
E_1 (GPa)	E_2 (GPa)	E_3 (GPa)	v_{12}	v_{13}	v_{23}	G_{12} (GPa)	G_{23} (GPa)	G_{31} (GPa)
54.9	11.4	11.4	0.26	0.26	0.29	4.4	4.4	4.4

Epoxy				Cohesive element				
E (GPa)	2.7	v	0.3	Mode I/II Strength (MPa)	23/33	Mode I/II Fracture toughness (N/m)	370/830	

2.2 *Damage modeland modeling strategy*

As reported in [Walter, Subhash, Sankar and Yen (2010)] and will be reported later in this paper, during the beginning stage of the SBS tests, 3D woven composite specimens underwent elastic deformation. As the loads increased, matrix cracks and delaminations developed.

The cohesive element associated with a bi-linear traction-separation law was selected for modeling both matrix cracks and delaminations. This damage law enables the traction between two surfaces to be expressed in terms of relative displacement and stiffness:

$$
\sigma = (1-D)Kd
$$
$$
D = \begin{cases} 0, & d < d_0 \\ \frac{d_f(d-d_0)}{d(d_f-d_0)}, & d_0 < d < d_f \\ 1, & d_f < d \end{cases} \tag{1}
$$

where σ is the traction, K is stiffness, D is the damage variable, d is displacement, d is the displacement at damage initiation and d_f is the final displacement [Camanho, Dávila and de Moura (2003)]

Quadratic stress-based failure criterion and mixed mode strain energy release rate criterion were used for damage initiation and propagation, respectively, for both the matrix cracks and delaminations:

$$
\left\{\frac{<\sigma_n>}{\sigma_n^o}\right\}^2 + \left\{\frac{\sigma_s}{\sigma_s^o}\right\}^2 = 1 \tag{2}
$$

$$
\left\{\frac{G_I}{G_{IC}}\right\} + \left\{\frac{G_{II}}{G_{IIC}}\right\} = 1 \tag{3}
$$

where σ_n^o and σ_s^o are interfacial normal and shear strengths, and G_{IC} and G_{IIC} are the Mode I and Mode II critical energy release rates. Since the locations of cohesive elements, which would act as potential crack paths, should be defined a *priori*, it was necessary to predict reasonably the locations of expected cracks. The prediction for delaminations is straightforward as it would occur between adjacent plies or layers, while that for matrix crack is complex. Based on experimental observations by Walter et al. [Walter, Subhash, Sankar and Yen (2010)], some assumptions were made to determine the locations of potential cracks for the efficient use of cohesive elements as follows: i) Matrix cracks occur both within the fill tows and in the matrix pocket at the tensile bottom layer; ii) Only a single matrix crack is created and allowed to evolve along the principal stress direction; iii) The crack path is a straight-line; and iv) The effect of a matrix crack at the top-most compressive layer on delamination is negligible.
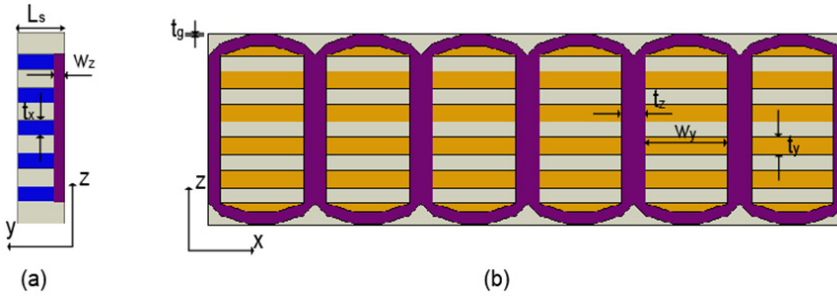
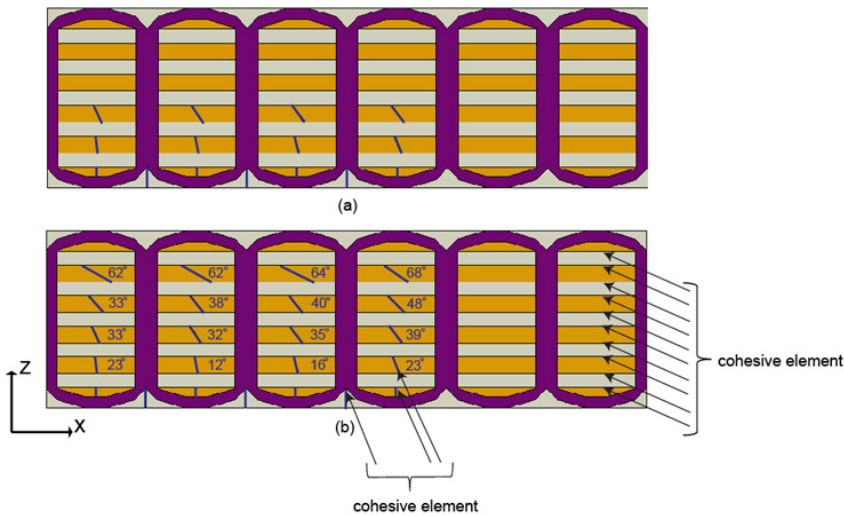Figure 2: Geometric parameter of RVE: (a) left side view and (b) front side view

Figure 3: Prediction of matrix cracks: The lines indicate potential crack paths (a) Principal stress directions in the tensile region (b) Principal stress directions in the entire regions

Formation of matrix cracks on the top layers of the beam required special treatment. In the beginning of loading the top side is under compression and no matrix cracks form. However, after delaminations initiated, there was a redistribution of stresses and the delaminated top layers develop tensile stresses and they became sites for initiation of matrix cracks. These locations were identified by analyzing principal stress directions from a preliminary FE analysis. Using the specimen without any damage (see Fig. 2) the principal directions at the centers of fill tows in the tensile region were found. In the subsequent FE model, cohesive elements for the matrix

cracks were implemented along the principal directions found in the previous step. Other cohesive elements for delaminations were simultaneously placed between layers so that the principal directions in the compressive region after delamination could be found. A similar FE analysis was performed using the specimen of Fig. 3(a) in which the load was applied until delaminations occurred so that redistributed stress fields could be obtained. In order to determine the principal stress directions in the weft yarns, stress values in all elements of the weft yarns were checked and appropriate principal stress directions were chosen for cohesive elements. The principal stress directions determined are shown in Fig. 3(b) over the entire specimen. Note that the angles shown in Fig. 3 were measured from the z-axis. As a result of consecutive finite element simulations the final configuration of Fig. 3(b) was reached which was then used to study of delamination damage of the 3D woven composites.

2.3   *Finite element model for 2D plain woven laminates (2DPL)*

A plain woven laminate (2DPL) with stacking sequence $\left[(0^{pw}/45^{pw})_2/\bar{0}^{pw}\right]_S$ was also analyzed, where the superscript *pw* denotes plain-woven. The 2DPL was chosen for comparison with the 3D woven composites, and thus investigating the effect of z-yarns on delamination behavior. For the sake of simplicity of FE simulations, each plain woven layer was homogenized as an orthotropic material and one-half of the beam was modeled using eight-node plane strain elements. The material properties of the homogenized plain-woven layer are listed in Table 3 [Xiao, Gama and Gillespie Jr. (2007)]. The material properties for $\pm45^{pw}$ could be obtained using coordinate transformation.

Table 3: Elastic properties for the plain woven composites[34]

$E_1=E_2$ (GPa)	E_3 (GPa)	$G_{13}=G_{23}$ (GPa)	G_{12} (GPa)	$\nu_{13}=\nu_{23}$	ν_{12}
27.5	11.8	2.14	2.9	0.4	0.11

The creation of matrix cracks and placement of cohesive elements in the 2DPL specimens were similar to the procedures used for the 3D woven laminates. Our approach was confirmed by the experimental observation that a single matrix crack tended to occur inside weft yarns of the $0/90^{pw}$ [Walter, Subhash, Sankar and Yen (2010)]. However, the tensile cracks in the matrix pocket of outermost layer seen in the 3D woven composites were not observed in plain woven laminates, and hence they were not introduced in the 2DPL specimens. Furthermore, transverse shear stress vanishes at the free surface. Therefore, cohesive elements for possible matrix

cracks were placed in the three inner homogenized layers of $0/90^{pw}$ as shown in Fig. 4. Principal stress directions were found in locations corresponding to the centers of fill tows using the same procedure as in 3D woven composites. The possible matrix crack directions used in this simulation are shown in Fig.4.
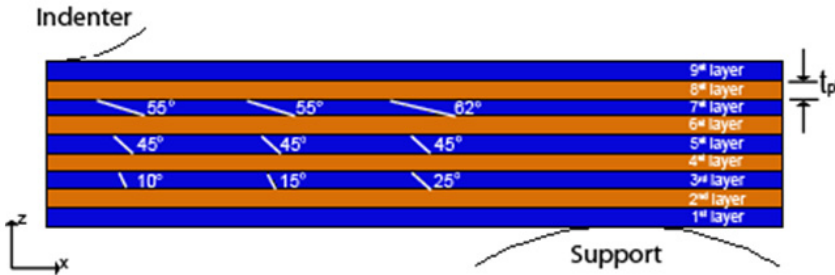

Figure 4: Implementation of cohesive element on homogenized 2D plain woven composite

A parametric study varying Mode I/Mode II interlaminar fracture toughness (370/830 N/m, 1,000/2,000 N/m and 1,000/3,300 N/m) was performed in order to investigate the effect of interlaminar fracture toughness on the global behavior and the evolving damage pattern in 2DPL specimens. These studies were referred to as Case I, Case II and Case III (see Table 4), respectively.

Table 4: Parameters for the cohesive element in baseline composite model

	σ_{max} (MPa)	G_{Ic} (N/m)	τ_{max} (MPa)	G_{IIc} (N/m)
Case I	23	370	33	830
Case II	23	1000	33	2000
Case III	23	1000	33	3300

3 Results and discussions

3.1 3D woven composites

The force and displacement at the indenter were calculated using the FE simulations. The force for a given displacement could be a proper measure to examine the macroscopic behavior of the specimen. The results for both the SY3W and the

DY3W are shown in Fig.5. Two force-displacement curves from the experiments [Walter, Subhash, Sankar and Yen (2010)] are also plotted for comparison. Note the two experimental curves of the same SY3W specimens show slightly different behavior after damage initiation indicating a large variability in specimens. The solid lines indicate the result from the FE model. Since the same properties for the cohesive elements were used and most configurations remained the same except for the thickness of z-yarns in the simulation of SY3W and DY3W specimens, it could be inferred that the difference between two FE simulations (solid curves in Fig.5) resulted from the effect of z-yarns on delamination. The peak load of the DY3W was higher than that of the SY3W. This revealed that z-yarns could delay the damage initiation point. Moreover, the forces beyond the peak loads between the two cases were quite different. The SY3W showed the abrupt force-drop right after the peak load whereas the force-drop in the DY3W was fairly small. Additionally the SY3W had another peak load followed by the sudden force drop again, which did not occur in the DY3W. These characteristics agree well with experimental results shown in Fig. 5.
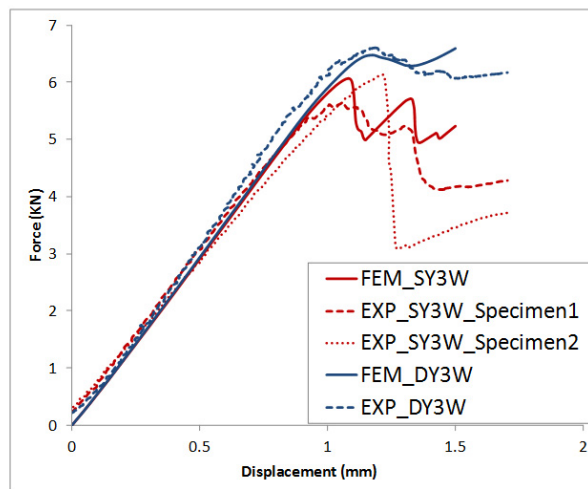

Figure 5: Force-displacement curves of the SY3W and the DY3W

The variation of strain energy and damage energy as a function of indenter displacement obtained from the FE analyses are shown in Fig. 6. The strain energy represents the recoverable elastic energy stored in the specimen at any given instant. The damage energy is the unrecoverable energy dissipated by the cohesive elements. It was seen that the sudden force-drop in the load-deflection diagram

corresponded to sudden increase in damage energy. One can note that the damage energy in the DY3W specimen increased steadily without any abrupt damage process or loss of stiffness. From these figures it was clear that z-yarns could enhance damage resistance and tolerance. However, optimum amount of z yarn should be used so that there is no deterioration in the in-plane properties of the composite [Song, Snakar, Subhash and Yen (2012); Rao, Sankar and Subhash (2009)].
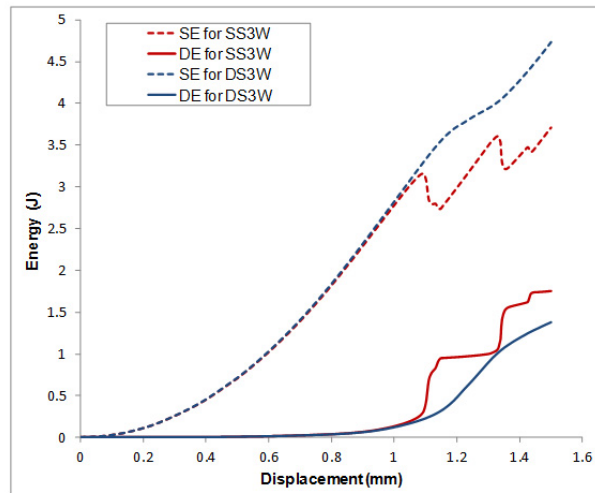

Figure 6: Strain energy and damaged energy versus displacement curves of the SY3W and the DY3W. SE and DE indicate strain energy and damage energy, respectively.

3.2 *Plain woven laminated composites*

Unlike 3D woven composites, only one configuration, but with various cohesive parameters, was considered in studying the 2DPL. Although the same properties for cohesive element as the 3D woven composites were initially used for the 2DPL, interlaminar fracture toughness values would be different since woven laminated composites have higher fracture toughness value than unidirectional fiber composites due to the undulation of yarns or crimps [Kalarikkal, Sankar and Ifju (2006)]. The force versus displacement curves at the indenter due to three different interlaminar fracture toughness values are plotted in Fig. 7. Out of the three sets of interlaminar fracture toughness values used, the force-displacement curve of Case III with the highest fracture toughness exhibited load-displacement behavior similar to experimental results as shown in Fig.7. Lower fracture toughness values

(cases I and II) resulted in different damage pattern and produced different load-displacement curves.
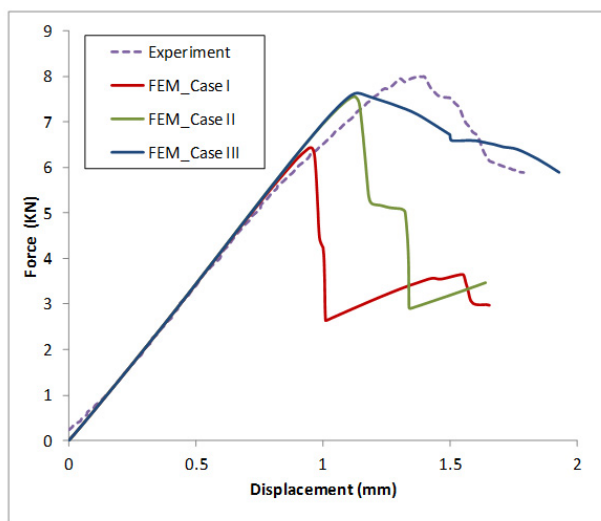

Figure 7: Force-displacement curves of the 2DPL

The distinction among these three force-displacement curves is apparent. As the fracture toughness values were increased, the peak loads also increased and the rate of force drop just beyond the peak load became moderate. If the interlaminar cracks propagate mainly without other delaminations the forces will decrease rapidly. As seen in Fig. 7 the rapid force drops in the Case I and Case II were attributed to the damage that occurred with very small increment of displacement and could be clearly identified with the damage energy variation in Fig. 8. Sudden increase of the damage energy was accompanied by sudden loss of the strain energy as well. But the damage energy of Case III increased gradually along with the increase of the strain energy. These variations of global responses were highly dependent on how damage evolved. By observing the history of damage development, it was possible to gain insight into delamination damage behavior of composites. Once delamination occurred from the matrix crack, it would propagate and in the end reach the free end of the specimen (b-2and c-2 in Fig. 9). The propagation of the crack to the free end caused the force to decrease abruptly. After a complete delamination developed over the region from matrix cracks to the end of the specimen, the force increased with displacement and the strain energy was stored until the state of stress in another interlaminar region satisfied with the criterion for crack initiation and propagation. Then the force would decrease suddenly again
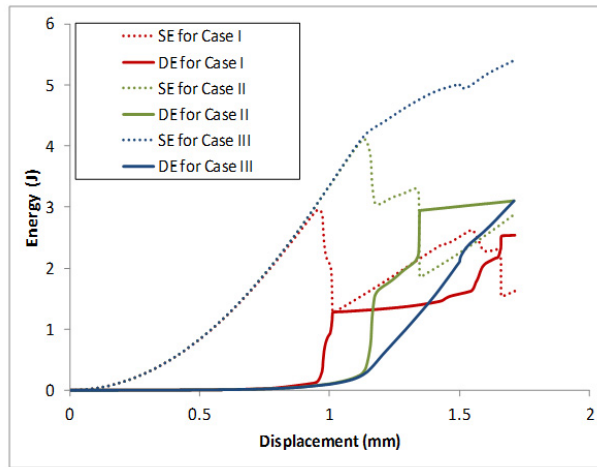
Figure 8: Strain energy and damage energy versus displacement curves of the 2DPW. SE and DE indicate strain energy and damage energy, respectively.
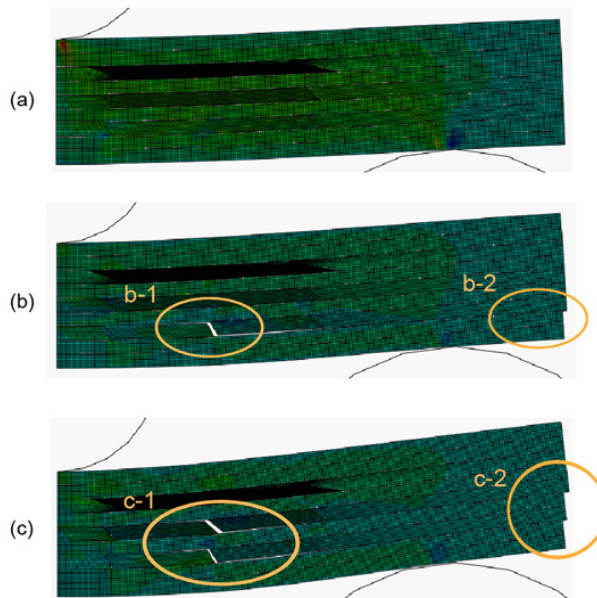

Figure 9: Damage evolution of the 2DPL - Case I: (a) d=0.8mm (b) d=1.1mm (c) d=1.7 mm
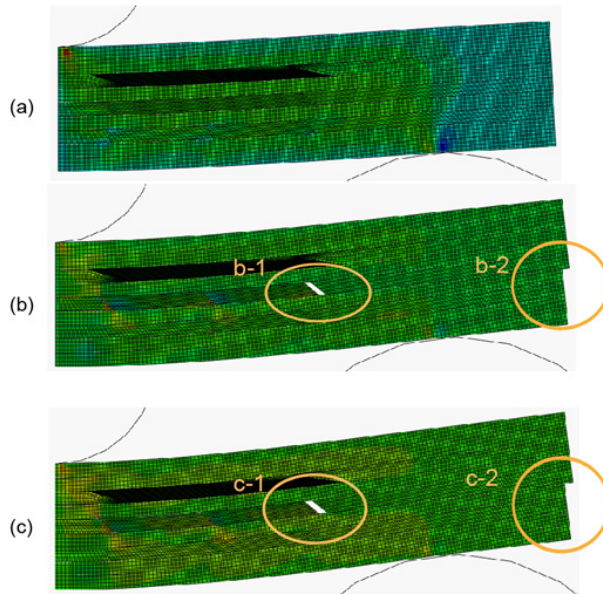
Figure 10: Damage evolution of the 2DPL - Case II: (a) d=1mm (b) d=1.5mm (c) d=1.75 mm
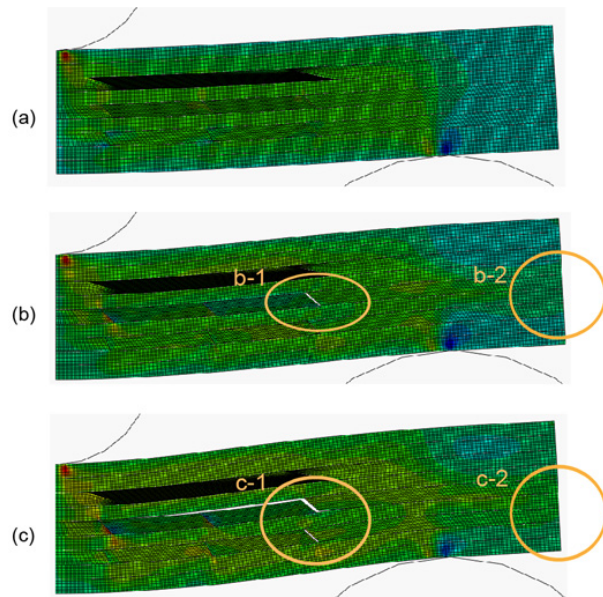

Figure 11: Damage evolution of the 2DPL - Case III: (a) d=1mm (b) d=1.5mm (c) d=1.75 mm
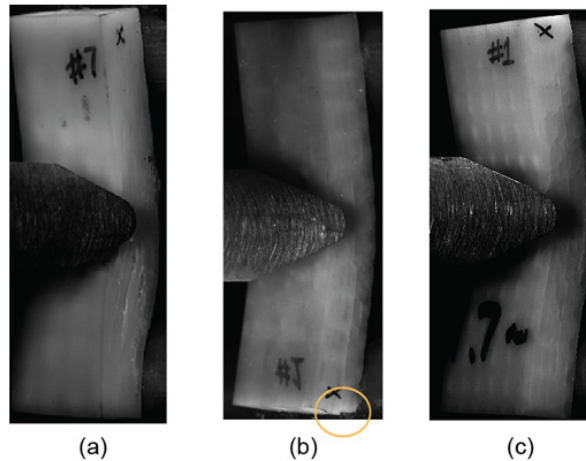
Figure 12: Delamination patterns in the composites: (a) the 2DPL (b) the SY3W (c) the DY3W

as shown in the Case I of Figs. 7 and 9(c). Case II showed that the resistance to crack propagation increased with the interlaminar fracture toughness. Although the interlaminar crack was created from a matrix crack at a different location from the Case I and propagated up to the end of the specimen, there was a region where the rate of force drop became slow (Fig. 7). Further increase in interlaminar fracture toughness (Case III) changed the tendency of crack propagation totally. High resistance against cracks kept the interlaminar delamination from propagating. Before a delamination reached to the end of specimen, another delamination occurred. This caused a gradual force drop instead of an abrupt drop in the Case I and II (Figs. 7 and 11). The relationships between the damage patterns in Figs. 9 through 11 and the force-displacement curves in Fig. 7 were similar to the test results of Walter [Walter (2011)]. It could be observed that the crack propagation of the SY3W reached the end of the specimen and resulted in the force-displacement curve in Fig. 5, while the 2DPL and the DY3W didn't allow delaminations to propagate to the end of the specimens or other delaminations occurred at the same time and thus they resulted in gradual force drop as shown in Fig 12. It should be noted that Fig. 12 has been obtained from low velocity impact tests but exhibited similar damage patterns as quasi-static tests demonstrating that quasi-static indentation tests could provide insight into damage development due to impact loading in laminated 3D composites.

From these results, it was possible to identify the role of z-yarns on delamina-

tion. Z-yarns provided constraints to reduce the relative displacement between two layers, thus enhancing the resistance against crack propagation. Thus the z-yarns resulted in higher apparent interlaminar fracture toughness.

4   Summary and Conclusions

The effect of z-yarns on damage tolerance of 3D woven composites was studied by simulating the Short Beam Shear test specimens. Based on the previous experimental observations that tensile or transverse matrix cracks develop in the matrix pocket between z-yarn crowns and inside wept yarns, a simplified FEM approach using cohesive elements was introduced. The cohesive elements associated with bi-linear damage model were placed along the principal stress direction for the matrix cracks and between layers for delaminations. The FE model incorporating RVE model and plane strain boundary condition provided reasonable results to understand the role of z-yarns and inherent interlaminar fracture toughness.

From the FE simulations of the SY3W and the DY3W specimens, it was found that appropriate volume fraction of z-yarns could enhance the damage resistance and tolerance by preventing two neighboring layers from being separated. These conclusions agreed well with the result from the end-notch flexure (ENF) specimen of 3D woven composites by Pankow et al. [Pankaw, Waas, Yen and Ghiorse (2011)]. In the case of the 2DPL, crimps or undulations would interrupt the propagation of delamination cracks providing better damage tolerance than the SY3W where the volume fraction of z-yarn is insufficient. However, the DY3W had superior damage tolerance compared to the 2DPL and the SY3W.

From the parametric study for the 2DPL, it was concluded that the prevention of crack growth along an entire interface without other damages was a key factor in enhancing damage tolerance. When damages occurred in different layers before the delamination propagated in the entire specimen, more energy was dissipated in various interlaminar damage mechanisms thus increasing the damage tolerance of the laminated composite structure.

Finally, the FE models for two types of 3D woven composites and a parametric study for 2D plain woven composites provided a good correlation between the amount of z-yarns and interlaminar fracture toughness They help in the understanding of role of z-yarn in enhancing apparent fracture toughness, which would be very practical in the design of composite structures.

ratory. The authors also would liketo thank Dr. Bazle Z. (Gama) Haque at the University of Delaware for the personal communication about the volume fraction of yarns in 3D woven composites.

References

Advanced Materials (2013): http://www.agy.com/technical_info/graphics_PDFs/Advanced_Materials.pdf

Applied Poleramic. (2013): http://www.appliedpoleramic.com/specs/vartm_rtm.php

Belytschko, T.; Cracie, R.; Ventura, G. (2009): A review of extended/generalized finite element methods for material modeling. *Modeling Simulation Material Sci Eng*, vol.17, no.4, pp.1-24.

Byrd, L.W.; Birman, V. (2005): The estimate of the effect of z-pins on the strain release rate,fracture and fatigue in a composite co-cured z-pinned double cantilever beam. *CompositeStructures*, vol.68, pp. 53–63.

Camanho, P.P.; Dávila, C.G.; de Moura, M.F. (2003): Numerical simulation of mixed-mode progressive delamination in composite materials. *J Composite Material*, vol.37, no.16, pp. 1415–1438.

Cartie D.D.R. (2000): Effect of Z-fibreson the delamination behaviour of carbon-fibre/epoxy Laminates *Ph.D.thesis*, Cranfield University, UK.

Chamis, C.C.; Handler, L.M.; Manderscheid, J. (2007): Composite Nanomechanics: A Mechanistic Properties Prediction. *NASA/TM—2007-214673*, Glenn Research Center, Cleveland, OH.

Chen,L; Sankar, B.V.; Ifju, P.G. (2002): A new mode I fracture test for composites with translaminar reinforcements. *Composites Science & Technology,* vol.62, pp. 1407-1414.

Dantuluri, V; Maiti, S; Geubelle, P.H.; Patel, R.; Kilic. H. (2007): Cohesive modeling of delamination in Z-pin reinforced composite laminates. *Composites Science & Technology*, vol.67, pp. 616-631.

Grassi, M; Zhang, X. (2003): Finite element analyses of mode I interlaminar delamination in z-fibre reinforced composite laminates. *Composites Science & Technology,* vol.63, pp.1815-1832.

Hallett, SR.; Jiang, WG.; Khan, B.; Wisnom, MR (2008): Modelling the interaction between matrix cracksand delamination damage in scaled quasi-isotropic specimens. *Composites Science & Technology*, vol.68, pp. 80-89.

Huang, H.; Waas, A.M. (2009): Compressive response of Z-pinned woven glass fiber textile composite laminates: Modeling and computations. *Composite Science*

& Technology, vol.69, no.14, pp. 2338-2344.

Jain L.K.; Mai Y.W. (1998): On the effect of stitching on Mode I delamination toughness of laminated composites. *Composites Science & Technology*, vol.58, pp. 829-837.

Kalarikkal S.; Sankar BV.; Ifju PG. (2006): Effect of Cryogenic Temperature on the Fracture Toughness of Graphite/Epoxy Composites. *ASME Journal of Engineering Materials and Technology,* vol.128, no.2, pp. 151-157.

Ling, D.S.; Yang,Q.D.; Cox, B. (2009): An augmented finite element method for modeling arbitrary discontinuities in composite materials. *Intl J Fracture*, vol.156, pp. 53-73.

Mabson, GE.; Deobald, LR. (2000): Design curves for 3D reinforcement laminated double cantilever beams. *Proc of ASME Int. Mechanical Eng. Congress and Expo.*, pp. 89-99.

Nishikawa, M.; Okabe, T.; Takeda, N. (2007): Numerical simulation of interlaminar damage propagationin CFRP cross-ply laminates under transverse loading. *International Journal of Solids and Structures* , vol.44, pp. 3101–3113.

Okabe, T.; Yashiro, S. (2012): Damage detection in holed composite laminates using an embedded FBG sensor. *Composites Part A*, vol.43, pp. 388-397.

Pankow M, Waas AM, Yen CF, Ghiorse S (2011): Resistance to delamination of 3D woven textile composites evaluated using End Notch Flexure (ENF) tests: Cohesive zone based computational results *Composites Part A,* vol.42, no.12, pp. 1863-1872.

Ratcliffe, J,G.;O'brien, T.K. (2004): Discrete spring model for predicting delamination growth in z-fiber reinforced DCB specimens. *NASA/TM-2004-213019*, ARL-TR-3190.

Rao, M.P.; Sankar, B.V.; Subhash, G. (2009): Effect of z-yarns on the stiffness and strength of three-dimensional woven composites. *Composites Part B,* vol.40, pp. 540-551.

Ratcliffe, J,G.; O'brien, T.K. (2004): Discrete spring model for predicting delamination growth in z-fiber reinforced DCB specimens. *NASA/TM-2004-213019*, ARL-TR-3190.

Ratcliffe, J.G.; Kruger, R.A. (2006): Finite Element Analysis for Predicting Mode I-Dominated Delamination Growth in Laminated Structure with Through-Thickness Reinforcement. In: *Proceedings of American Society for Composites –* 21stAnnual Technical Conference, Dearborn, Michigan.

Robinson, P.; Das, S. (2004): Mode I DCB testing of composite laminates reinforced with z-direction pins: A simple model for the investigation of data reduction

strategies. *Engg. Fracture Mech,* vol.71, pp. 345-364.

Sankar, B.V.; Sun, C.T. (1986): Low-Velocity Impact Damage in Graphite-Epoxy Laminates Subjected to Tensile Initial Stresses. *AIAA Journal*, vol.24, no.3, pp. 470-471.

Sankar, B.V., Hu, S. (1991): Dynamic delamination propagation in composite beams, *J Composite Materials,* vol.25, no.11, pp. 1414-1426.

Sankar, B.V.; Sharma, S,K. (1997): Mode II delamination toughness of stitched graphite/epoxy textile composites. *Composites Science &Technology*, 57, pp. 729-737.

Sankar, B.V.;Dharmapuri, S.M. (1998): Analysis of a Stitched Double Cantilever Beam. *J Composite Materials,* vol.32, pp. 2204-2225.

Sankar, B.V.; Zhu, H. (2000): Effect of stitching on the low-velocity impact response of delaminated composite beams. *Composites Science & Technology*, vol.60, pp. 2681-2691.

Song, M.C.; Sankar, B.V.; Subhash, G.; Yen, C.F. (2012): Analysis of mode I delamination of z-pinned composites using a non-dimensional analytical model. *Composites Part B,* vol.43, pp. 1776-1784.

Sridhar, N.; Massabo, R.; Cox, B.N.; Beyerlein, I.J. (2002): Delamination dynamics in through-thickness reinforced laminates with application to DCB specimen delaminated composite beams. *Int J Fracture*, vol.118, pp. 119-144.

Walter, T.R.; Subhash, G.; Sankar, B.V.; Yen, C.F. (2010): Monotonic and cyclic short beam shear response of 3D woven composites. *Composites Science & Technology*, vol.70, pp. 2190–2197.

Walter T.R. (2011): Characterization of delamination in 3d woven composites under static and dynamic loading. *PhD thesis*. Univ. of Florida

Wisnom, M.R. (2010): Modelling discrete failures in composites with interface elements. *Composites PartA*, vol.41, pp. 795-805.

Xiao,JR.;Gama,B.A.;Gillespie Jr., JW (2007): Progressive and delamination delamination in plain weave S-2 glass/SC-15 composites under quasi-static punch-shear loading. *Composite Structures,* vol.78, pp. 182-196.

Zhou, Z.Q.; Fang, X.J.; Cox, B.N.; Yang, Q.D. (2010): The evolution of a transverse intra-ply crack coupled to delamination cracks. *Intl J Fracture*, vol.165, pp. 77-92.